Evidence for a Long-Range Component in the Pion Emission Source in Au + Au Collisions at $\sqrt{s_{NN}} = 200$ GeV

S. S. Adler,[5] S. Afanasiev,[18] C. Aidala,[5] N. N. Ajitanand,[44] Y. Akiba,[21,39] J. Alexander,[44] R. Amirikas,[13] L. Aphecetche,[46] S. H. Aronson,[5] R. Averbeck,[45] T. C. Awes,[36] R. Azmoun,[45] V. Babintsev,[16] A. Baldisseri,[10] K. N. Barish,[6] P. D. Barnes,[28] B. Bassalleck,[34] S. Bathe,[31] S. Batsouli,[9] V. Baublis,[38] A. Bazilevsky,[40,16] S. Belikov,[17,16] Y. Berdnikov,[41] S. Bhagavatula,[17] J. G. Boissevain,[28] H. Borel,[10] S. Borenstein,[26] M. L. Brooks,[28] D. S. Brown,[35] N. Bruner,[34] D. Bucher,[31] H. Buesching,[31] V. Bumazhnov,[16] G. Bunce,[5,40] J. M. Burward-Hoy,[27,45] S. Butsyk,[45] X. Camard,[46] J.-S. Chai,[19] P. Chand,[4] W. C. Chang,[2] S. Chernichenko,[16] C. Y. Chi,[9] J. Chiba,[21] M. Chiu,[9] I. J. Choi,[53] J. Choi,[20] R. K. Choudhury,[4] T. Chujo,[5] P. Chung,[44] V. Cianciolo,[36] Y. Cobigo,[10] B. A. Cole,[9] P. Constantin,[17] M. Csanád,[12] T. Csörgő,[22] D. d'Enterria,[46] G. David,[5] H. Delagrange,[46] A. Denisov,[16] A. Deshpande,[40] E. J. Desmond,[5] A. Devismes,[45] O. Dietzsch,[42] O. Drapier,[26] A. Drees,[45] R. du Rietz,[30] A. Durum,[16] D. Dutta,[4] Y. V. Efremenko,[36] K. El Chenawi,[50] A. Enokizono,[15] H. En'yo,[39,40] S. Esumi,[49] L. Ewell,[5] D. E. Fields,[34,40] F. Fleuret,[26] S. L. Fokin,[24] B. D. Fox,[40] Z. Fraenkel,[52] J. E. Frantz,[9] A. Franz,[5] A. D. Frawley,[13] S.-Y. Fung,[6] S. Garpman,[30,*] T. K. Ghosh,[50] A. Glenn,[47] G. Gogiberidze,[47] M. Gonin,[26] J. Gosset,[10] Y. Goto,[40] R. Granier de Cassagnac,[26] N. Grau,[17] S. V. Greene,[50] M. Grosse Perdekamp,[40] W. Guryn,[5] H.-Å. Gustafsson,[30] T. Hachiya,[15] J. S. Haggerty,[5] H. Hamagaki,[8] A. G. Hansen,[28] E. P. Hartouni,[27] M. Harvey,[5] R. Hayano,[8] N. Hayashi,[39] X. He,[14] M. Heffner,[27] T. K. Hemmick,[45] J. M. Heuser,[45] M. Hibino,[51] J. C. Hill,[17] W. Holzmann,[44] K. Homma,[15] B. Hong,[23] A. Hoover,[35] T. Ichihara,[39,40] V. V. Ikonnikov,[24] K. Imai,[25,39] D. Isenhower,[1] M. Ishihara,[39] M. Issah,[44] A. Isupov,[18] B. V. Jacak,[45] W. Y. Jang,[23] Y. Jeong,[20] J. Jia,[45] O. Jinnouchi,[39] B. M. Johnson,[5] S. C. Johnson,[27] K. S. Joo,[32] D. Jouan,[37] S. Kametani,[8,51] N. Kamihara,[48,39] J. H. Kang,[53] S. S. Kapoor,[4] K. Katou,[51] S. Kelly,[9] B. Khachaturov,[52] A. Khanzadeev,[38] J. Kikuchi,[51] D. H. Kim,[32] D. J. Kim,[53] D. W. Kim,[20] E. Kim,[43] G.-B. Kim,[26] H. J. Kim,[53] E. Kistenev,[5] A. Kiyomichi,[49] K. Kiyoyama,[33] C. Klein-Boesing,[31] H. Kobayashi,[39,40] L. Kochenda,[38] V. Kochetkov,[16] D. Koehler,[34] T. Kohama,[15] M. Kopytine,[45] D. Kotchetkov,[6] A. Kozlov,[52] P. J. Kroon,[5] C. H. Kuberg,[1,28,*] K. Kurita,[40] Y. Kuroki,[49] M. J. Kweon,[23] Y. Kwon,[53] G. S. Kyle,[35] R. Lacey,[44] V. Ladygin,[18] J. G. Lajoie,[17] A. Lebedev,[17,24] S. Leckey,[45] D. M. Lee,[28] S. Lee,[20] M. J. Leitch,[28] X. H. Li,[6] H. Lim,[43] A. Litvinenko,[18] M. X. Liu,[28] Y. Liu,[37] C. F. Maguire,[50] Y. I. Makdisi,[5] A. Malakhov,[18] V. I. Manko,[24] Y. Mao,[7,39] G. Martinez,[46] M. D. Marx,[45] H. Masui,[49] F. Matathias,[45] T. Matsumoto,[8,51] P. L. McGaughey,[28] E. Melnikov,[16] F. Messer,[45] Y. Miake,[49] J. Milan,[44] T. E. Miller,[50] A. Milov,[45,52] S. Mioduszewski,[5] R. E. Mischke,[28] G. C. Mishra,[14] J. T. Mitchell,[5] A. K. Mohanty,[4] D. P. Morrison,[5] J. M. Moss,[28] F. Mühlbacher,[45] D. Mukhopadhyay,[52] M. Muniruzzaman,[6] J. Murata,[39,40] S. Nagamiya,[21] J. L. Nagle,[9] M. Nagy,[12] T. Nakamura,[15] B. K. Nandi,[6] M. Nara,[49] J. Newby,[47] P. Nilsson,[30] A. S. Nyanin,[24] J. Nystrand,[30] E. O'Brien,[5] C. A. Ogilvie,[17] H. Ohnishi,[5,39] I. D. Ojha,[50,3] K. Okada,[39] M. Ono,[49] V. Onuchin,[16] A. Oskarsson,[30] I. Otterlund,[30] K. Oyama,[8] K. Ozawa,[8] D. Pal,[52] A. P. T. Palounek,[28] V. Pantuev,[45] V. Papavassiliou,[35] J. Park,[43] A. Parmar,[34] S. F. Pate,[35] T. Peitzmann,[31] J.-C. Peng,[28] V. Peresedov,[18] C. Pinkenburg,[5] R. P. Pisani,[5] F. Plasil,[36] M. L. Purschke,[5] A. K. Purwar,[45] J. Rak,[17] I. Ravinovich,[52] K. F. Read,[36,47] M. Reuter,[45] K. Reygers,[31] V. Riabov,[38,41] Y. Riabov,[38] G. Roche,[29] A. Romana,[26,*] M. Rosati,[17] P. Rosnet,[29] S. S. Ryu,[53] M. E. Sadler,[1] N. Saito,[39,40] T. Sakaguchi,[8,51] M. Sakai,[33] S. Sakai,[49] V. Samsonov,[38] L. Sanfratello,[34] R. Santo,[31] H. D. Sato,[25,39] S. Sato,[5,49] S. Sawada,[21] Y. Schutz,[46] V. Semenov,[16] R. Seto,[6] M. R. Shaw,[1,28] T. K. Shea,[5] T.-A. Shibata,[48,39] K. Shigaki,[15,21] T. Shiina,[28] C. L. Silva,[42] D. Silvermyr,[28,30] K. S. Sim,[23] C. P. Singh,[3] V. Singh,[3] M. Sivertz,[5] A. Soldatov,[16] R. A. Soltz,[27] W. E. Sondheim,[28] S. P. Sorensen,[47] I. V. Sourikova,[5] F. Staley,[10] P. W. Stankus,[36] E. Stenlund,[30] M. Stepanov,[35] A. Ster,[22] S. P. Stoll,[5] T. Sugitate,[15] J. P. Sullivan,[28] E. M. Takagui,[42] A. Taketani,[39,40] M. Tamai,[51] K. H. Tanaka,[21] Y. Tanaka,[33] K. Tanida,[39] M. J. Tannenbaum,[5] A. Taranenko,[44] P. Tarján,[11] J. D. Tepe,[1,28] T. L. Thomas,[34] J. Tojo,[25,39] H. Torii,[25,39] R. S. Towell,[1] I. Tserruya,[52] H. Tsuruoka,[49] S. K. Tuli,[3] H. Tydesjö,[30] N. Tyurin,[16] H. W. van Hecke,[28] J. Velkovska,[5,45] M. Velkovsky,[45] V. Veszprémi,[11] L. Villatte,[47] A. A. Vinogradov,[24] M. A. Volkov,[24] E. Vznuzdaev,[38] X. R. Wang,[14] Y. Watanabe,[39,40] S. N. White,[5] F. K. Wohn,[17] C. L. Woody,[5] W. Xie,[6] Y. Yang,[7] A. Yanovich,[16] S. Yokkaichi,[39,40] G. R. Young,[36] I. E. Yushmanov,[24] W. A. Zajc,[9,†] C. Zhang,[9] S. Zhou,[7] S. J. Zhou,[52] and L. Zolin[18]

(PHENIX Collaboration)

[1]*Abilene Christian University, Abilene, Texas 79699, USA*
[2]*Institute of Physics, Academia Sinica, Taipei 11529, Taiwan*
[3]*Department of Physics, Banaras Hindu University, Varanasi 221005, India*

[4]Bhabha Atomic Research Centre, Bombay 400 085, India

[5]Brookhaven National Laboratory, Upton, New York 11973-5000, USA

[6]University of California - Riverside, Riverside, California 92521, USA

[7]China Institute of Atomic Energy (CIAE), Beijing, People's Republic of China

[8]Center for Nuclear Study, Graduate School of Science, University of Tokyo, 7-3-1 Hongo, Bunkyo, Tokyo 113-0033, Japan

[9]Columbia University, New York, New York 10027, USA
and Nevis Laboratories, Irvington, New York 10533, USA

[10]Dapnia, CEA Saclay, F-91191, Gif-sur-Yvette, France

[11]Debrecen University, H-4010 Debrecen, Egyetem tér 1, Hungary

[12]ELTE, Eötvös Loránd University, H - 1117 Budapest, Pázmány P. s. 1/A, Hungary

[13]Florida State University, Tallahassee, Florida 32306, USA

[14]Georgia State University, Atlanta, Georgia 30303, USA

[15]Hiroshima University, Kagamiyama, Higashi-Hiroshima 739-8526, Japan

[16]IHEP Protvino, State Research Center of Russian Federation, Institute for High Energy Physics, Protvino, 142281, Russia

[17]Iowa State University, Ames, Iowa 50011, USA

[18]Joint Institute for Nuclear Research, 141980 Dubna, Moscow Region, Russia

[19]KAERI, Cyclotron Application Laboratory, Seoul, South Korea

[20]Kangnung National University, Kangnung 210-702, South Korea

[21]KEK, High Energy Accelerator Research Organization, Tsukuba, Ibaraki 305-0801, Japan

[22]KFKI Research Institute for Particle and Nuclear Physics of the Hungarian Academy of Sciences (MTA KFKI RMKI),
H-1525 Budapest 114, POBox 49, Budapest, Hungary

[23]Korea University, Seoul, 136-701, Korea

[24]Russian Research Center "Kurchatov Institute", Moscow, Russia

[25]Kyoto University, Kyoto 606-8502, Japan

[26]Laboratoire Leprince-Ringuet, Ecole Polytechnique, CNRS-IN2P3, Route de Saclay, F-91128, Palaiseau, France

[27]Lawrence Livermore National Laboratory, Livermore, California 94550, USA

[28]Los Alamos National Laboratory, Los Alamos, New Mexico 87545, USA

[29]LPC, Université Blaise Pascal, CNRS-IN2P3, Clermont-Fd, 63177 Aubiere Cedex, France

[30]Department of Physics, Lund University, Box 118, SE-221 00 Lund, Sweden

[31]Institut für Kernphysik, University of Muenster, D-48149 Muenster, Germany

[32]Myongji University, Yongin, Kyonggido 449-728, Korea

[33]Nagasaki Institute of Applied Science, Nagasaki-shi, Nagasaki 851-0193, Japan

[34]University of New Mexico, Albuquerque, New Mexico 87131, USA

[35]New Mexico State University, Las Cruces, New Mexico 88003, USA

[36]Oak Ridge National Laboratory, Oak Ridge, Tennessee 37831, USA

[37]IPN-Orsay, Universite Paris Sud, CNRS-IN2P3, BP1, F-91406, Orsay, France

[38]PNPI, Petersburg Nuclear Physics Institute, Gatchina, Leningrad Region, 188300, Russia

[39]RIKEN, The Institute of Physical and Chemical Research, Wako, Saitama 351-0198, Japan

[40]RIKEN BNL Research Center, Brookhaven National Laboratory, Upton, New York 11973-5000, USA

[41]Saint Petersburg State Polytechnic University, St. Petersburg, Russia

[42]Instituto de Física, Universidade de São Paulo, Caixa Postal 66318, São Paulo CEP05315-970, Brazil

[43]System Electronics Laboratory, Seoul National University, Seoul, South Korea

[44]Chemistry Department, Stony Brook University, SUNY, Stony Brook, New York 11794-3400, USA

[45]Department of Physics and Astronomy, Stony Brook University, SUNY, Stony Brook, New York 11794, USA

[46]SUBATECH (Ecole des Mines de Nantes, CNRS-IN2P3, Université de Nantes) BP 20722 - 44307, Nantes, France

[47]University of Tennessee, Knoxville, Tennessee 37996, USA

[48]Department of Physics, Tokyo Institute of Technology, Oh-okayama, Meguro, Tokyo, 152-8551, Japan

[49]Institute of Physics, University of Tsukuba, Tsukuba, Ibaraki 305, Japan

[50]Vanderbilt University, Nashville, Tennessee 37235, USA

[51]Advanced Research Institute for Science and Engineering, Waseda University, 17 Kikui-cho, Shinjuku-ku, Tokyo 162-0044, Japan

[52]Weizmann Institute, Rehovot 76100, Israel

[53]Yonsei University, IPAP, Seoul 120-749, Korea

Emission source functions are extracted from correlation functions constructed from charged pions produced at midrapidity in Au + Au collisions at $\sqrt{s_{NN}} = 200$ GeV. The source parameters extracted from these functions at low k_T give first indications of a long tail for the pion emission source. The source extension cannot be explained solely by simple kinematic considerations. The possible role of a halo of secondary pions from resonance emissions is explored.

Collisions between ultrarelativistic heavy ions can lead to extremely high energy-density nuclear matter [1]. The decay dynamics of this matter is strongly influenced by the nuclear equation of state (EOS) and possibly by a deconfined phase [2]. An emitting system which undergoes a strong first order phase transition is expected to show a much larger space-time extent than would be expected if the system remained in the hadronic phase throughout the collision process [3]. Indeed, several hydrodynamical calculations show such an increase for particle emission sources [3,4], provided hadronization does not occur via a supercooled state [5]. It has also been suggested that the shape of the emission source function can provide signals for a second order phase transition and whether or not particle emission occurs near to the critical end point in the QCD phase diagram [6].

Interferometry studies provide important information on the emission source function for particles produced in nuclear reactions ranging from elementary collisions [e^+e^- and $(\bar{p})pp$] to those involving very heavy ions [7–9]. Recent studies span the beam energies $\sqrt{s_{NN}} \sim$ 2–200 GeV [10–13]. A common theme for these papers is the extraction of the widths of emission source functions which are assumed to be Gaussian. Also, Coulomb effects on the correlation function are usually assumed to be separable [14]. Such an approach was followed earlier in an analysis which used the Bowler-Sinyukov 3D Hanbury Brown and Twiss (HBT) method to probe for a possible long-lived source [15]. The rms widths so obtained for each dimension of the source R_{long}, R_{side}, and R_{out} gave no evidence for such emissions, suggesting that the sound speed is not zero during an extended hadronization period.

In this Letter we exploit the model-independent imaging technique of Brown and Danielewicz [16,17] to make a more detailed study of both the shape and the space-time characteristics of the pion emission source function. The method uses a numerical calculation of the two particle wave function, which includes final-state interactions (FSI), to produce an inversion matrix that operates on the correlation function to produce the corresponding source function. The technique has been used to address only a few data sets [18,19] at relativistic beam energies.

Measurements were made with the PHENIX detector [20] at the Relativistic Heavy Ion Collider (RHIC). Charged pions were detected in the two central arms ($|\eta| \leq 0.35$). Track reconstruction was accomplished via pattern recognition using the drift chamber (DC) followed by two layers of multiwire proportional chambers with pad readout located at radii of 2, 2.5, and 5 m [20]. Particle momenta were measured with the resolution $\delta p/p = 0.7\% \oplus 1.0\% p$ (GeV/c). Very good pion identification (PID) was achieved with a 2σ cut about the pion peak in the squared-mass distribution for $p_T \lesssim 2.0$ GeV/c and $p_T \lesssim 1$ GeV/c in the time of flight (TOF) and the electromagnetic calorimeter (EMC), respectively. The event cen-

trality was determined using the PHENIX beam-beam counter and the zero degree calorimeter [21]. Approximately 22×10^6 Au + Au events were analyzed to study several centrality and p_T selections.

Two-pion interferometry correlations were obtained via the correlation function $C(q) = N_{\mathrm{cor}}(q)/N_{\mathrm{mix}}(q)$, where the numerator is the relative momentum distribution of particle pairs from the same event (foreground pairs) and the denominator is the relative momentum distribution of particle pairs obtained from mixed events (background pairs). Here, $q = \frac{1}{2}\sqrt{-(p_1 - p_2)^2}$ is half of the relative momentum between the two particles in the pair c.m. frame (PCMS). p_1 and p_2 are the momentum 4-vectors of each particle in the pair and $C(q) \equiv 1$ for large q values where final-state interactions are negligible. Track-pair cuts similar to those of Ref. [12] were applied to foreground and background pairs, respectively. That is, pairs
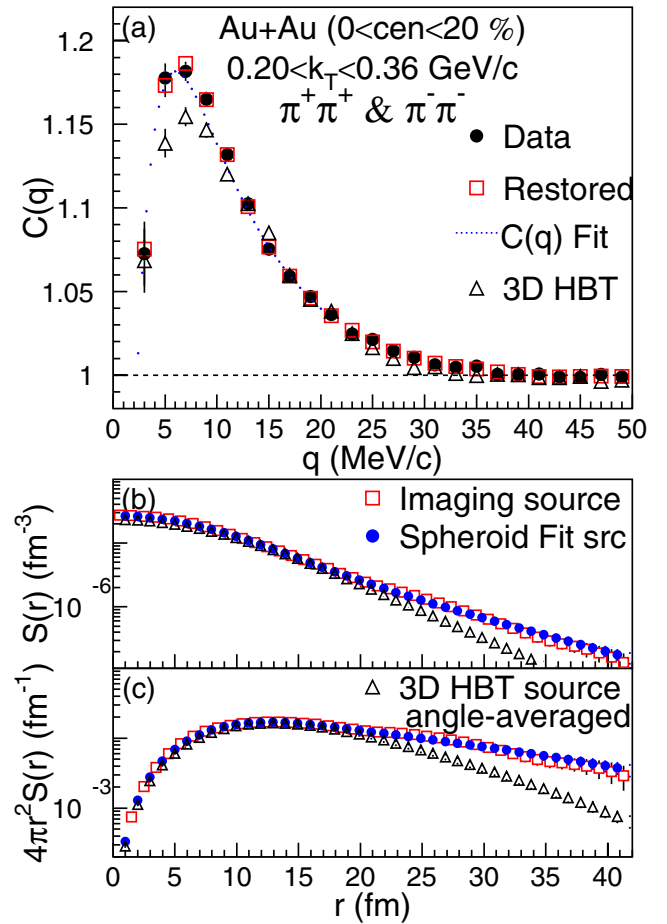

FIG. 1 (color online).   [(upper, (a)] (●) Correlation function, $C(q)$, for $\pi^+\pi^+$ and $\pi^-\pi^-$ pairs; (□) restored correlation from imaging technique; (dotted line) direct correlation fitting; (△) 1D angle-averaged correlation of 3D correlation function. (lower) 1D source function (b) $S(r)$ and (c) $4\pi r^2 S(r)$: (□) imaging; (●) spheroid fit to correlation function; (△) angle-averaging of 3D-Gaussian source function. Systematic errors are less than size of data points.

within 5 cm in the beam direction (ΔZ_{DC}) and 0.02 radians in azimuthal angle ($\Delta \phi_{DC}$) in the DC were eliminated from the pair sample to remove ghost tracks, and pairs within $0.0 < \Delta \phi_{DC} < 0.1$ radians for $\Delta Z_{DC} > 5$ cm were removed to avoid an inefficient region. The latter set of cuts were supplemented with the removal of pairs having a separation $\Delta R \leq 14$ cm and ≤ 16 cm in the TOF and EMC, respectively. Systematic variations of all of these cuts were explored to determine systematic error estimates; very little influence on the extracted correlation functions was found. Careful studies of the influence of momentum resolution on the correlation function were also made, as in [22]. The maximum effect was found to be ~0.4% change in the correlation function at low q values, so it was neglected.

The filled circles in Fig. 1(a) show the one-dimensional (1D) correlation function $C(q)$, for a centrality of $0\%-20\%$ and for $0.20 < k_T = \frac{1}{2}(p_{T,1} + p_{T,2}) < 0.36$ GeV/c. The characteristic enhancement for $q \lesssim 25$ MeV/c reflects a combination of Bose-Einstein statistics and the FSI between pion pairs. The correlation function is not Coulomb corrected because the FSI (including Coulomb but no strong interaction) is included in the imaging and fitting procedure as described below.

The 1D correlation function and source function $S(r)$ (the probability of emitting a pair of particles at a separation r in the PCMS frame) are related via the 1D Koonin-Pratt equation [23]:

$$C(q) - 1 = 4\pi \int dr r^2 K_0(q, r) S(r). \quad (1)$$

The angle-averaged kernel $K_0(q, r)$ encodes the FSI and is given in terms of the final-state wave function $\Phi_{\mathbf{q}}(\mathbf{r})$, as $K_0(q, r) = \frac{1}{2} \int d[\cos(\theta_{\mathbf{q},\mathbf{r}})][|\Phi_{\mathbf{q}}(\mathbf{r})|^2 - 1]$, where $\theta_{\mathbf{q},\mathbf{r}}$ is the angle between $\mathbf{q}$ and $\mathbf{r}$ [17]. The procedure for the inversion of Eq. (1) to obtain $S(r)$ is also given in Ref. [17].

The open squares in Fig. 1(b) show the source function obtained from the correlation function presented in Fig. 1(a). As a cross-check of the imaging procedure, a restored correlation function was generated via Eq. (1) with the extracted source function as input. The open squares and filled circles in Fig. 1(a) indicate excellent consistency between the measured and restored correlation functions. The 1D source function, cf. Fig. 1(b), points to a Gaussian-like pattern at small r and a previously unresolved "tail" at large r. The robustness of this tail was established via an extensive array of tests including its dependence on pair and PID cuts, and on momentum resolution; no variation outside of the stated error bars was found.

This new observation of a tail is made more transparent via a comparison with the source function constructed from the parameters (R_{long}, R_{side}, R_{out}, and λ), obtained in an earlier 3D HBT analysis [15]. The procedures outlined in Ref. [17] were employed to construct this source

function (see Fig. 1). The measured and 3D angle-averaged correlation functions differ for $q \lesssim 15$ MeV/c as do the respective source functions for $r \gtrsim 17$ fm. The imaged source function exhibits a more prominent tail than the angle-averaged 3D HBT source function. This difference could stem from the Gaussian shape assumption employed in the 3D HBT analysis. The 3D Gaussian fitting procedure by construction is sensitive only to the main component of $S(r)$, and thus would not be capable of resolving fine structure at small-q/large-r. Given the fact that the volume element increases quadratically with pair separation, this difference is considerable as shown in Fig. 1(c), where the radial probabilities $[4\pi r^2 S(r)]$ are compared. The open triangles in Fig. 1(a) clearly indicate that the differences in the source functions reflect an important disparity in the corresponding correlation functions for $q \lesssim 10$–15 MeV.

Parameters of the source function for different assumed shapes were extracted via direct fits to the correlation function. Filled circles in Figs. 1(b) and 1(c) show the source function obtained from such a fit for a spheroidal shape [17],

$$S(r) = \frac{\lambda R_{eff} \times e^{-(r^2/4R_T^2)} \text{erfi} \left(\frac{r}{2R_{eff}} \right)}{(8\pi R_T^2 R_0 r)}, \quad \text{for } R_0 > R_T, \quad (2)$$

where $R_{eff} = 1/\sqrt{(1/R_T^2 - 1/R_0^2)}$, R_T is the radius of the spheroid in two perpendicular spatial dimensions and $R_0 = a \times R_T$ is the radius in the third spatial dimension; a is a scale factor. The long axis of the spheroid is assumed to be oriented in the out direction of the Bertsch-Pratt coordinate system. The fraction of pion pairs which contribute to the source λ is given by the integral of the normalized source function over the full range of r.

The procedure for making a direct fit to the correlation function involves the determination of a set of values for the spheroid parameters of Eq. (2), which reproduce the observed correlation function when the resulting source function is inserted into Eq. (1). The minimization package MINUIT was used to minimize the χ^2 between the observed and calculated correlation function. The χ^2/ndf value so obtained was ~1. The dotted curve in Fig. 1(a) shows the fit to the data. The resulting source function shown in Figs. 1(b) and 1(c) indicates very good agreement with that obtained via the imaging technique. This shape parametrization is not unique; an essentially indistinguishable source was also obtained for a fit performed with a Gaussian plus modified exponential [24] shape. The simpler spheroid parametrization was chosen for the discussion below.

The spheroidal source function [Eq. (2)] can be approximated by a short-range Gaussian source $S_{sr}(r)$;

$$S_{sr}(r) \sim \lambda e^{-r^2[(1/6R_T^2) + (1/12R_0^2)]}/(8\pi \sqrt{\pi} R_T^2 R_0), \quad (3)$$

for small r, and a long-range source $S_{lr}(r)$ for

$r \gg 2R_T R_0 / \sqrt{R_0^2 - R_T^2}$ given by

$$S_{\text{lr}}(r) \sim \lambda R_0 e^{-r^2/4R_0^2} / [4\pi\sqrt{\pi}(R_0^2 - R_T^2)r^2]. \quad (4)$$

Thus, the emission source shown in Figs. 1(b) and 1(c) can be interpreted to reflect a short-range Gaussian source of radius $R_{\text{sr}} = \sqrt{3R_T^2 R_0^2/(2R_0^2 + R_T^2)} = R_T\sqrt{3a^2/(2a^2 + 1)}$ and a long-range tail of extended space-time extent $R_{\text{lr}} = R_0$. The fraction of pairs associated with these sources $\lambda_{\text{sr}} = \lambda a^2[3/(2a^2 + 1)]^{3/2}$ and $\lambda_{\text{lr}} = (\lambda - \lambda_{\text{sr}})$ are obtained from Eq. (3) and the conservation of pairs, respectively.

Source functions were extracted via imaging and spheroid fits for several k_T and centrality selections, in order to map the regions in k_T and centrality where the long-range tail is prominent. Representative results are shown in Fig. 2 for the indicated cuts. The experimental and restored correlation functions, compared in Figs. 2(a) and 2(b), indicate good agreement within the statistics, as do the corresponding source functions shown in Figs. 2(c) and 2(d).

Figure 3 gives a more complete summary of the extracted source parameters. Systematic errors obtained via variations of pair cuts in the analysis are 0.12 fm, 1.0 fm, 0.35, and 0.03 for R_{sr}, R_{lr}, a, and λ, respectively. The centrality and k_T dependence of the rms radius of the short-range source R_{sr} is similar (within 10%) to that obtained for R_{long} and R_{side} in an earlier analysis [15],

cf. Figs. 3(a) and 3(d). The long-range source shows an effective radius $R_{\text{lr}} = a \times R_T$, which is $\sim$2–3.5 times R_{sr}. The ratio $R_{\text{lr}}/R_{\text{sr}}$ is also maximal for low k_T and the most central collisions. The fraction of pairs exhibiting these characteristics is given by the λ values shown in Figs. 3(c) and 3(f); for central collisions, maximum prominence is shown for low k_T pairs.

A central question is the origin of the long-range contribution to the emitting source. Instantaneous freeze-out of a source with $R_{\text{out}}/R_{\text{side}} \sim 1$ in the longitudinal comoving system (LCMS) would give a maximum kinematic boost so that $R_{\text{lr}} = R_{\text{out}} = \gamma \times R_T$ in the PCMS. Thus, the values for a and γ, shown in Fig. 3(b), can be directly compared. At low k_T, γ is seen to be significantly less than a. Thus, a simple kinematic transformation from the LCMS to PCMS cannot account for the observed source parameters at this k_T.

Could a composite particle emission source comprised of a central core and a halo of long-lived resonances account for the observations? For such emissions, the pairing between pions from the core and secondary pions from the halo is expected to dominate the long-range emissions [25]. If it is assumed that this halo includes only ω decay ($c\tau \sim 24$ fm), one may compare the ω yield with a simple estimate of the fraction of pion pairs associated with the short- and long-range sources. Using the a and γ values in Fig. 3(b), $\lambda_{\text{sr}} \sim 0.22$–0.32,
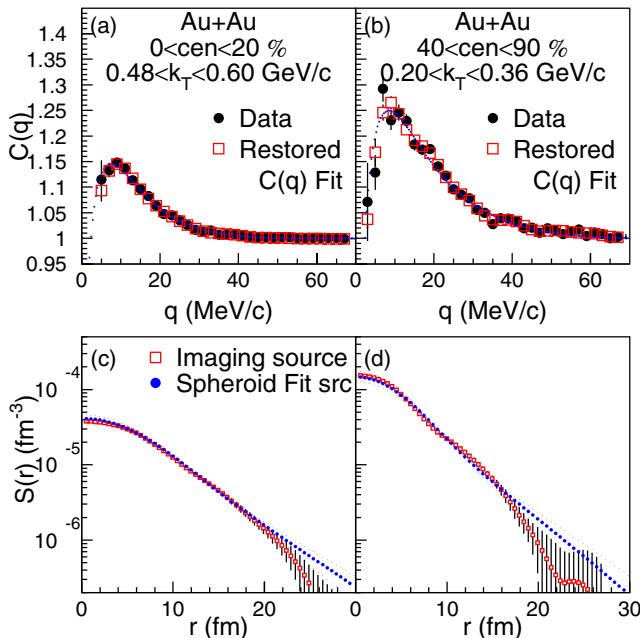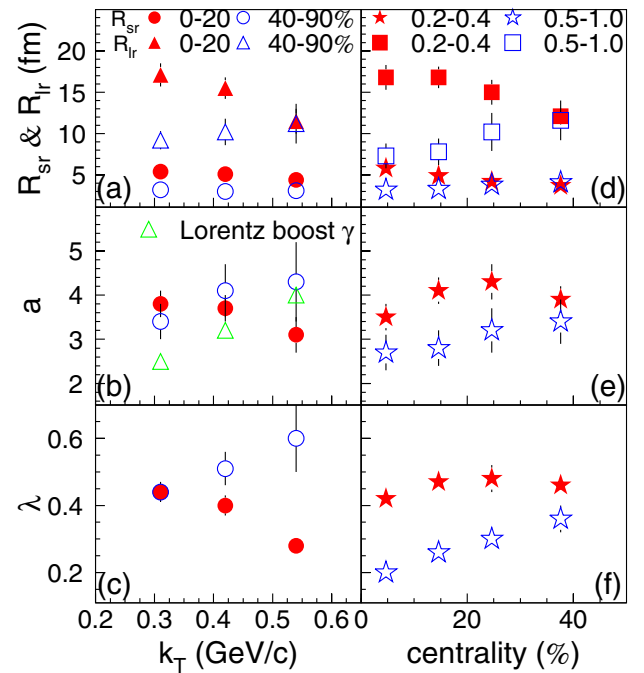

FIG. 2 (color online). (upper) Correlation functions, $C(q)$, for $\pi^+\pi^+$ and $\pi^-\pi^-$ pairs and (lower) corresponding source functions, $S(r)$ for (a), (c) high k_T most central collisions; (b), (d) low k_T peripheral collisions. Error bars indicate statistical errors with symbols as in Fig. 1.

FIG. 3 (color online). (left) k_T dependence of extracted spheroidal source parameters for pion source functions (a) R_{sr}, R_{lr}, (b) a, and (c) λ for (filled symbols) most central collisions; (open symbols) peripheral collisions. (right) Centrality dependence of same parameters for (★) low k_T (0.2–0.4 GeV/c); (☆) high k_T (0.5–1.0 GeV/c).

$\lambda_{\text{lr}} \sim 0.23$–$0.13$, and $\lambda_{\text{lr}}/\lambda_{\text{sr}} \sim 0.4$–$1.0$ for the lowest k_T. The preliminary values for $\omega/\pi^- = 0.1$ from Ref. [26] give an estimate for $\lambda_{\text{lr}}/\lambda_{\text{sr}} \sim 2 \times 0.1/\sqrt{\lambda_{\text{sr}}} \sim 0.35$–$0.43$ which lies at the lower end of the estimates obtained from the source parameters. (A significant change in the value for ω/π^- would alter this conclusion.) Therefore, it is plausible that a maximal kinematic boost combined with a halo of ωs could account for $\lambda_{\text{lr}}/\lambda_{\text{sr}}$. However, the steep centrality dependence of the radius of the long-range source inferred from Figs. 3(d) and 3(e) is not compatible with an essentially flat dependence expected for significant ω resonance contribution.

In summary, we have made the first extraction of the full 1D emission source function for pions in Au + Au collisions at RHIC ($\sqrt{s_{NN}} = 200$ GeV). This source function points to separate but prominent contributions from short-range emissions and a long-range tail of larger space-time extent than has been previously observed. This tail cannot be explained solely by simple kinematic considerations associated with a frame transformation from the LCMS to the PCMS. Further studies are required to determine the origin of this tail and whether or not it is related to a phase transition.

*Deceased.
†PHENIX Spokesperson.
Email address: zajc@nevis.columbia.edu

[1] K. Adcox *et al.*, Nucl. Phys. **A757**, 184 (2005).
[2] E. V. Shuryak, Nucl. Phys. A **750**, 64 (2005).
[3] S. Pratt, Phys. Rev. Lett. **53**, 1219 (1984).
[4] D. Teaney, J. Lauret, and E. V. Shuryak, Phys. Rev. Lett. **86**, 4783 (2001).
[5] T. Csorgo *et al.*, Phys. Lett. B **333**, 494 (1994).
[6] T. Csorgo, S. Hegyi, T. Novak, and W. A. Zajc, nucl-th/0512060.
[7] E. V. Shuryak, Phys. Lett. **44B**, 387 (1973).
[8] U. Heinz *et al.*, Annu. Rev. Nucl. Part. Sci. **49**, 529 (1999).
[9] T. Csorgo, Heavy Ion Physics **15**, 1 (2002).
[10] M. A. Lisa *et al.*, Annu. Rev. Nucl. Part. Sci. **55**, 357 (2005).
[11] C. Adler *et al.*, Phys. Rev. Lett. **87**, 082301 (2001).
[12] K. Adcox *et al.*, Phys. Rev. Lett. **88**, 192302 (2002).
[13] J. Adams *et al.*, Phys. Rev. Lett. **91**, 262301 (2003).
[14] Y. Sinyukov *et al.*, Phys. Lett. B **432**, 248 (1998).
[15] S. S. Adler *et al.*, Phys. Rev. Lett. **93**, 152302 (2004).
[16] D. A. Brown *et al.*, Phys. Lett. B **398**, 252 (1997).
[17] D. A. Brown and P. Danielewicz, Phys. Rev. C **64**, 014902 (2001).
[18] S. Y. Panitkin *et al.*, Phys. Rev. Lett. **87**, 112304 (2001).
[19] P. Chung *et al.*, Phys. Rev. Lett. **91**, 162301 (2003).
[20] K. Adcox *et al.*, Nucl. Instrum. Methods Phys. Res., Sect. A **499**, 469 (2003).
[21] K. Adcox *et al.*, Phys. Rev. C **69**, 024904 (2004).
[22] M. D. Baker *et al.* (E802 Collaboration), Nucl. Phys. **A610**, 213c (1996).
[23] S. E. Koonin, Phys. Lett. **70B**, 43 (1977).
[24] P. Chung *et al.*, Nucl. Phys. **A749**, 275 (2005).
[25] S. Nickerson, T. Csorgo, and D. Kiang, Phys. Rev. C **57**, 3251 (1998).
[26] W. Broniowski *et al.*, Acta Phys. Hung. A **22**, 159 (2005).